Tracking the changes of iron solubility and air pollutants traces as African dust transits the Atlantic in the Saharan dust outbreaks

Sergio Rodríguez [a,b,c,*], Joseph M. Prospero [d], Jessica López-Darias [c,e,f], María-Isabel García-Alvarez [a,e], Paquita Zuidema [d], Silvia Nava [g], Franco Lucarelli [g,h], Cassandra J. Gaston [d], Luis Galindo [e,f], Elisa Sosa [a]

[a] Izaña Atmospheric Research Centre, AEMET, Tenerife, Spain
[b] Experimental Station of Arid Zones, EEZA CSIC, Almería, Spain
[c] Institute of Natural Products and Agrobiology, IPNA CSIC, Tenerife, Spain
[d] Rosenstiel School of Marine and Atmospheric Science, University of Miami, USA
[e] Department of Chemistry, University of La Laguna, Tenerife, Spain
[f] General Service of Support to Research, SEGAI, University of La Laguna, Tenerife, Spain
[g] Physics Department, University of Florence, Firenze, Italy
[h] Istituto Nazionale di Fisica Nucleare, Firenze, Italy

HIGHLIGHTS

- Iron solubility increases from ~0.7% to 4.7% as Saharan dust fronts transit from Africa to the Americas.
- Dust, heavy fuel oil combustion and atmospheric processing are identified as sources of soluble iron.
- Fresh dust accounts for 63, 43 and 9% of soluble iron in Tenerife, Barbados and Miami.
- Aged dust accounts for 26, 45 and 74% of soluble iron in Tenerife, Barbados and Miami.
- Oil combustion accounts for 10, 12 and 16% of soluble iron in Tenerife, Barbados and Miami.

GRAPHICAL ABSTRACT
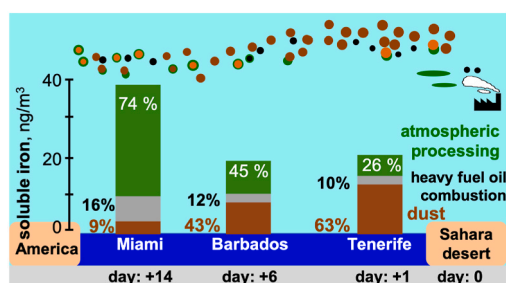
ARTICLE INFO

ABSTRACT

We studied the solubility, in real sea water, of iron present in the African dust outbreaks that traverse the Atlantic. Based on measurements of soluble iron (sFe) and aerosol chemistry, we found iron solubilities within the range of 0.4–1.8% in Tenerife, 0.4–3.1% in Barbados and 1.6–12% in Miami. We apportioned the concentrations of sFe between the three sources and processes that we identified: (1) dust, (2) heavy fuel oil combustion emissions, associated with an excess of vanadium and nickel, and (3) atmospheric processing, which is influenced by acidic pollutants. We tracked the propagation of the dust-front of the African dust outbreaks across the Atlantic, which are associated with dust peak events at the impacting sites. During the westward transport across the Atlantic, the contribution to sFe from dust decreased (63%, 43% and 9% in Tenerife, Barbados and Miami, respectively), whereas the contribution due to atmospheric processing increased (26%, 45% and 74% in Tenerife, Barbados and Miami, respectively). In these Saharan-dust outbreaks, the concentrations of sFe due to heavy fuel

---

oil combustion were significantly lower (mostly < 5 ng/m^3) than those in the polluted marine atmosphere (10–200 ng/m^3). The overall results are consistent with the idea that the mixing of dust with acid pollutants increases the solubility of iron during the African-dust outbreaks that traverse the Atlantic.

1. Introduction

Marine microorganisms account for $\sim$ half of Earth's primary productivity, i.e. the conversion of carbon from carbon dioxide to organic molecules via photosynthesis and chemosynthesis, a process that also replenishes the oxygen budget (Chapman, 2013). This process requires nutrients to support the growth of primary producers. In many regions of the open ocean, atmospheric deposition is the main supplier of those nutrients. Nitrogen and, to a lesser extent, phosphorus have historically been identified as limiting macronutrients (Falkowski, 1998; Moore et al., 2013). Iron is a limiting micronutrient for phytoplankton, especially in the high-nitrate, low-chlorophyll (HNLC) regions, which account for 30% of the oceans, particularly in the Southern Ocean and the equatorial and subarctic Pacific (Mahowald et al., 2018). The atmospheric deposition of Fe is estimated to support 30–50% of global export productivity, whereas that of nitrogen, silicon and phosphorus is estimated to support 3–5%, ~0.2% and ~0.1% of global export productivity (Duce et al., 2008; Jickells et al., 2014; Krishnamurthy et al., 2010), respectively. It is thought that desert dust was the main source of iron to the ocean in pre-industrial times. Ice core records suggest that increased dust inputs to the ocean may have reduced atmospheric CO_2 in glacial versus interglacial periods, linked to iron modulated primary productivity (Martínez-Garcia et al., 2009; Ridgwell and Watson, 2002).

Since the advent of the Anthropocene, huge amounts of chemicals have been transferred from the atmosphere to the ocean, where they act as nutrients (N, Fe and P), toxins (e.g. Pb, Cu and Hg) and pH regulators (carbon dioxide), with implications on ocean ecosystems, carbon sequestration and climate (Duce et al., 2009; Mahowald, 2011). The composition of the marine biota community and its biological productivity may be altered due to the inputs of co-limiting trace metal (e.g. Zn, Co and Mn; Ahlgren et al., 2014; Browning et al., 2014; Saito et al., 2008), whereas other elements (e.g. Cu) may be toxic for plankton (Jordi et al., 2012; Paytan et al., 2009). Fertilization experiments have found that increased growth rates linked to iron-addition also shift the community composition and the biomass accumulation (de Baar, 2005; Boyd et al., 2007). The response of these marine communities to such deposition of chemicals has also implications in the Ocean Deoxygenation (Ito et al., 2016).

It is generally accepted that the solubility of Fe (i.e., the ratio of soluble to total Fe, %) deposited in the ocean will affect its bioavailability (Schulz et al., 2012). The solubility of Fe in dust samples collected from soil is typically low (as low as 0.1%), i.e. much lower than that observed in the Fe contained in the atmospheric aerosols (~0.45% for dust and up to 80% for other aerosols; Schroth et al., 2009; Shi et al., 2009, 2012). Mineralogy has been found to play an important role on the inherent solubility of dust (Gaston, 2020; Journet et al., 2008). High values of Fe solubility in the atmospheric aerosols are attributed to the emissions of pyrogenic particles (Ito et al., 2019) and atmospheric processing (Gaston, 2020; Kanakidou et al., 2018). The Fe solubility of pyrogenic particles may reach values of ~20% for coal and for biomass burning fly ashes and ~80% for oil combustion, specially low grade fuels, as heavy fuel oil (HFO) (Ito, 2013; Wang et al., 2015). The high Fe solubility in fly ashes linked to HFO combustion is attributed to ferric sulphate and to aggregated nanocrystals of magnetite (Fu et al., 2012; Schroth et al., 2009), formed at temperatures >800 °C, followed by sulphuric acid condensation (Sippula et al., 2009). In coal fly ash, rapid acid chemistry on aluminosilicates glasses formed at high temperature combustion followed by cooling process contributes to quick Fe leaching (Chen et al., 2012). During transport, atmospheric processing can increase the solubility of iron containing minerals (Kanakidou et al., 2018)

by a set of processes still under research, including proton-promote dissolution due to the reaction of iron with inorganic and organic acids (Ito, 2015; Longo et al., 2016; Meskhidze, 2003; Shi et al., 2009), ligand-controlled dissolution due to the presence of organic ligands, as oxalate, that bind Fe in organic soluble complexes (Meskhidze et al., 2017; Wozniak et al., 2013) and photo-reduction involing the reduction of Fe(III) to Fe(II) (Chen and Grassian, 2013; Johnson and Meskhidze, 2013; Paris et al., 2011). Variability in pH and acidic conditions contributes to the formation of reactive iron nanoparticles in cloud (Shi et al., 2009). Several factors affect the efficiency of these iron dissolution processes including particle size (Baker and Jickells, 2006; McDaniel et al., 2019), dust mineralogy including the mineral form of iron present and the presence of semiconductor minerals, light, and the presence and types of acids, inorganic and organic ligads (Fu et al., 2010; Hettiarachchi and Rubasinghege, 2020; Rubasinghege et al., 2012; Wiederhold et al., 2006). In cloud processing of dust and pH variability contribute to the neo-formation of iron nanoparticles that increases iron reactivity (Shi et al., 2009).

Source-specific values of Fe solubility have been used in atmospheric transport models for quantifying the natural and anthropogenic inputs of soluble Fe to the ocean (e.g. $\sim$ 0.45% for dust and 20%, 80% and 18% for coal, oil and biomass-burning fly ashes, respectively (Ito, 2013; Ito and Feng, 2010; Johnson and Meskhidze, 2013; Wang et al., 2015). Atmospheric chemical transport models have also incorporated acid dissolution schemes, based on laboratory experiments and kinetic process, in which the initial values of Fe solubility in combustion fly ashes and dust aerosol evolves depending on mineralogy, meteorology, pH, solar radiation and the mixing with inorganic (sulphuric, nitric and hyper-chloric) and organic (oxalate) acids (Ito and Feng, 2010; Ito and Xu, 2014; Johnson and Meskhidze, 2013).

The increasing volume of experimental data is providing a broad view on the variability range of iron solubility over the ocean (Baker et al., 2016; Baker and Jickells, 2017; Ingall et al., 2018), which shows that there are still major uncertainties regarding the sources and atmospheric processes contributing to the enhancements in Fe solubility (Aguilar-Islas et al., 2010; Ingall et al., 2018; Ito et al., 2019; Kanakidou et al., 2018; Mahowald et al., 2018; Meskhidze et al., 2016b; Raiswell et al., 2017). Models suggest that the amount of soluble Fe deposited in the ocean may have doubled since the industrial revolution (0.06–0.12 Tg/y^{-1}), not only because of the emissions of pyrogenic iron but also because of the acid dissolution of dust (Ito and Shi, 2016). There is a clear need to develop tools for apportioning measured soluble iron between the different sources and for assessing the relative importance of atmospheric processes in contributing to increasing iron solubility (Baker et al., 2016; Mead et al., 2013).

The majority of dissolved iron in the oceans is bound to iron-binding ligands or colloids (Buck et al., 2015). In the surface of the tropical and subtropical North Atlantic ocean, underlying the Saharan-dust plume, dissolved iron is predominantly found as colloids (Fitzsimmons et al., 2015). In contrast, no such preference is observed in regions where dust concentrations are low such as the Southern Ocean (Boye et al., 2010) and the Subarctic Pacific (Nishioka et al., 2001), where deposition of soluble iron is dominated by combustion sources (Ito, 2015).

We present the results of an experiment focused on studying the change of iron solubility after African dust plumes had crossed the Atlantic. We tracked the propagation of dust outbreaks across the North Atlantic and studied the evolution of aerosols composition, iron solubility and source-tracers. Our objective was to measure soluble iron concentrations before and after transit, to link changes to the impact of specific source types, and to identify the processes that might lead to
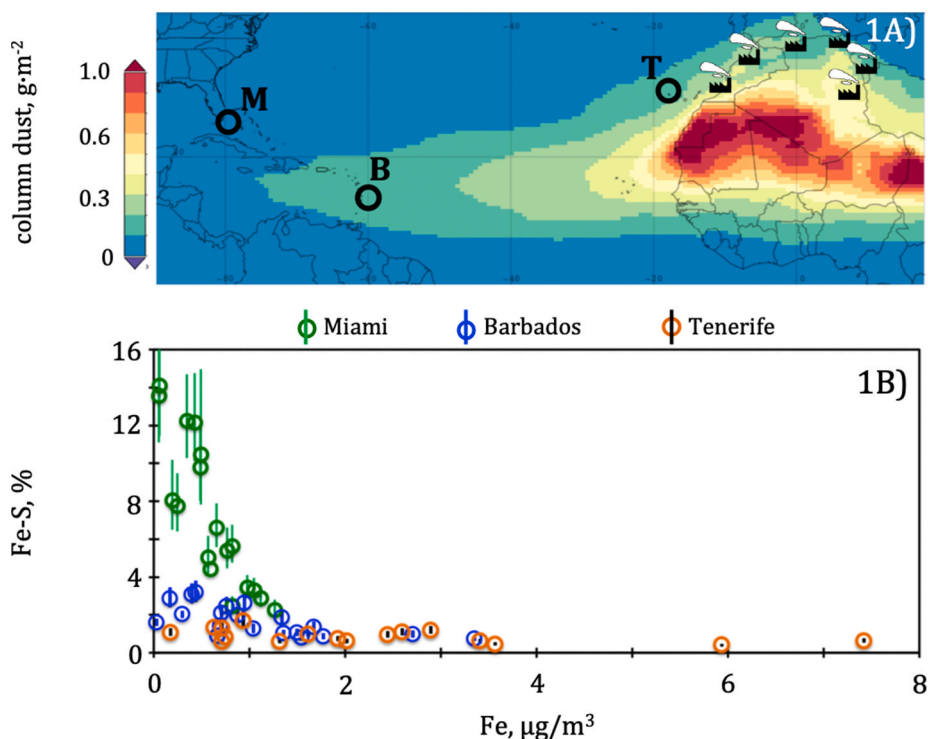
Fig. 1. A) Measurements sites (Tenerife - T, Barbados – B and Miami - M) illustrated in the average MERRA-2 column dust in July and August 2015. The industrial areas of North Africa are highlighted (Rodríguez et al., 2011). B) Iron solubility (Fe–S) versus iron in the samples collected in Tenerife, Barbados and Miami during July and August 2015. Vertical barr of each dot represents the uncertainity interval of each iron solubility data.

changes in iron solubility.

2. Materials and methods

2.1. Sampling and chemical determinations

From 30 June to September 1, 2015 we collected daily samples of aerosols in three sites of the North Atlantic: (i) at Izaña Observatory in Tenerife island (28.308 °N, 16.500 °W), located at ~2400 m above sea level (m.a.s.l.), directly exposed to the dusty air arriving from the inner Sahara, (ii) Ragged Point, on Barbados (13.165 °N, 59.432 °W), ~45 m. a.s.l., exposed to the easterly trade winds blowing in the tropical central North Atlantic and (iii), Virginia Key (25.732 °N, 80.162 °W), an island 4 km east off the coast at Miami, ~30 m.a.s.l., directly exposed to the trade winds arriving from the tropical Atlantic and the eastern Caribbean. The three sites have produced multi-decadal dust records (Prospero, 1999, 2003; Rodríguez et al., 2015; Zuidema et al., 2019).

At the three sites, the samples were collected on Whatman™-41 cellulose filters at the flow rates of 30 m³/h in Tenerife and 40 m³/h in Barbados and Miami. A characterization of the blank of these filters and detection limits, within the frame of the GEOTRACES program, was presented by Morton et al. (2013). The analytical methods that we used were described previously (Rodríguez et al., 2012) and in the Supplementary Material (SM). These analyses allowed the determinations of dust (Prospero, 1999), ions and cations (Na⁺, SO₄⁻, NO₃⁻, NH₄⁺ and Cl⁻, where ' = ' indicate charge −2 for sulphate; Prospero, 1999) and elemental composition (Na, Mg, Al, Si, S, Cl, K, Ca, Ti, V, Cr, Mn, Fe, Ni, Cu, Zn, Sr; Calzolai et al., 2015; Lucarelli et al., 2014, 2018). We determined soluble iron in 55 samples collected before, during and after dust peak events. Soluble iron from the three sites was determined by extracting the samples in seawater (pH = 8.1) collected offshore in Northern Tenerife and filtered through a 0.45 μm filter (Ravelo-Pérez et al., 2016). The extraction of the soluble iron in seawater collected in the same site avoid uncertanites linked to heterogeneity in seawater composition, particularly organic ligands (Buck et al., 2006).
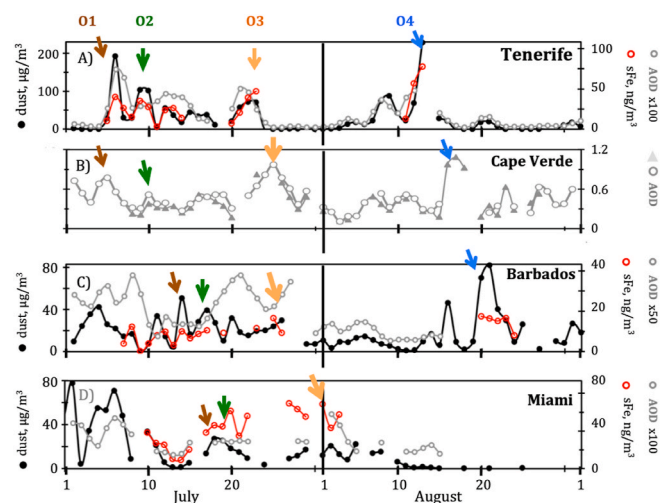

Fig. 2. Dust and Aerosol Optical Depth (AOD) in summer 2015. Concentrations of dust (in μg/m³) and soluble iron (sFe, in ng/m³) at Tenerife (A), Barbados (C) and Miami (D). AOD at Tenerife (A), Cape Verde (B, Sao Vicente site – grey triangles and Calhau - grey dots), Barbados (C) and Miami (D). Arrows O1 to O4 mark the location of the dust-front linked to the four identified dust outbreaks that transited the Atlantic. O4 didn't reach Miami.

The uncertainty linked to soluble iron concentrations was estimated based on replicate analyses of the leaching that yielded a average precision of ±7% (n = 7 samples). The uncertainty linked to PIXE was determined (in ng/m³) for each sample (considering X-ray counting statistics, areal densities of certified standards and aerosol sampling parameters); the average ratio of this uncertainty to the concentration value was ~10% for Fe and 14% for Al. Because of their low concentration, this ratio was higher for trace elements: ~47% for V > 5 ng/m³ and ~30% for Ni > 0.9 ng/m³, and higher for lower V and Ni
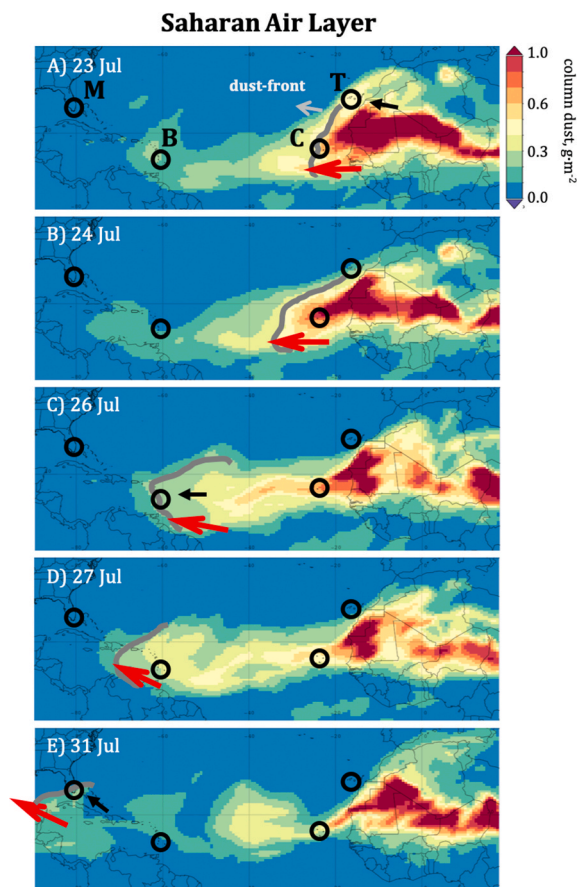
Saharan Air Layer

Fig. 3. Westward propagation of dust, from 23rd to July 31, 2015, highlighting the location of the dust front (red arrow and grey line) during the outbreak O3 and the impact (black arrow) at Tenerife (T), Barbados (B) and Miami (M). C: Cape Verde. Dust is represented as dust column loading (kg·m^{-2}) according to the MERRA-2 model. (For interpretation of the references to colour in this figure legend, the reader is referred to the Web version of this article.)

concentrations. Iron solubility (Fe–S) was determined as:

$$Fe - S = \left(\frac{sFe}{Fe}\right) \cdot 100 \tag{1}$$

The uncertainty interval (Fe-S$_{min}$, Fe-S$_{max}$) of each Fe–S data was determined considering the uncertainty of sFe (ΔsFe) and Fe (ΔFe):

$$Fe - S_{min} = \left(\frac{sFe - \Delta sFe}{Fe + \Delta Fe}\right) \cdot 100 \tag{2a}$$

$$Fe - S_{max} = \left(\frac{sFe + \Delta sFe}{Fe - \Delta Fe}\right) \cdot 100 \tag{2b}$$

The width of the lower side (Fe–S – Fe-S$_{min}$) and upper side (Fe-S$_{max}$ - Fe–S) of the uncertainty interval, with respect to the Fe–S central position, was used to estimate Fe–S uncertainty. The average ratio of this uncertainty to the concentration value, in the whole data set, was 18% for Fe–S data. This uncertainty is higher than that of sFe and Fe due to the amplification effect of the ratios (equations (2a and 2b)). The same analysis yields values of 94% for the V/Al ratios, due to the low concentrations of V and the amplification effect of equations (2) and (3) ratios. The uncertainty intervals for sFe, Fe, Fe–S and the V/Al ratio are shown in some plots (Figs. 1B and 4A-4B).

2.2. Complementary data

Complementary data were used to track dust transport across the

Atlantic: (i) Aerosol Optical Depth (AOD) measurments of the AERONET network at the three sampling sites and in two sites in Cape Verde (Calhau and Sao Vicente), and (ii) surface dust concentrations (µg/m^3) and column dust (kg/m^2) obtained with MERRA-2 model (Barkley et al., 2019; Gelaro et al., 2017). AOD is a measure of the attenuation (extintion) of the sunlight, caused by the atmospheric aerosols, when light propagates from the top of the atmosphere to the Earth surface, directly related to column dust load.

2.3. Source apportionment of soluble iron

We used two approaches, the minimum ratio and the minimum border line, to apportion soluble iron between the different sources. Theses two methods were previously used for segregating the contributions of primary and secondary sources of organic aerosols (Turpin and Huntzicker, 1995; Na et al., 2004) and of ultrafine particles (Kulmala et al., 2016; Reche et al., 2011; Rodríguez and Cuevas, 2007). As far as we know, this methodology is applied for the first time to soluble iron.

We used the excess of vanadium, with respect to its content soil dust content, as a proxy to trace HFO combustion emissions (Ault et al., 2010; Sedwick et al., 2007; Trapp et al., 2010a). Thus, the vanadium linked to dust (V$_d$) and to HFO combustion (V$_c$) was determined as:

$$V = V_d + V_c \tag{3}$$

$$V_d = \begin{cases} V, & \left(\frac{V}{Al}\right) \leq \left(\frac{V}{Al}\right)_d \\ \left(\frac{V}{Al}\right)_d \cdot Al, & \left(\frac{V}{Al}\right) > \left(\frac{V}{Al}\right)_d \end{cases} \tag{4}$$

$$V_c = \begin{cases} 0, & \left(\frac{V}{Al}\right) \leq \left(\frac{V}{Al}\right)_d \\ V - V_d, & \left(\frac{V}{Al}\right) > \left(\frac{V}{Al}\right)_d \end{cases} \tag{5}$$

where, (V/Al)$_d$ is the maximum value of the vanadium to aluminium ratio in North African dust. Several V/Al ratios observed in soils have been published, ranging from (dimensionless mass ratios) 0.9·10^{-3} (Taylor and Mclennan, 1985), to 1.17·10^{-3} (Mason, 1966; Taylor, 1964) and to 1.3·10^{-3} (Rudnick and Gao, 2003) for the global average in the Earth crust and 1.13·10^{-3} in North African soil desert dust (Eglinton et al., 2002). When applying the minimum ratio method, we used a value (V/Al)$_d$ = 1.15·10^{-3}. Thus, we assumed that the V/Al in Saharan dust may experience a certain variability, with a maximum equal to this threshold value. In aerosol dust samples with a V/Al ratio < (V/Al)$_d$, the measured vanadium is attributed to dust (equation (4a)) and V$_c$ = 0 (equation (5a)). In samples with a V/Al ratio > (V/Al)$_d$, V$_d$ is calculated using the (V/Al)$_d$ (equation (4b)), whereas V$_c$ is calculated as the excess of vanadium with respect to this (V/Al)$_d$ threshold (equation (5b)). When applying the lower border line method, the characteristic (V/Al)$_d$ above which the iron solubility increases, linked to HFO combustion emissions, was experimentally determined for each site, as detailed below.

Analytical data used in this study and the source apportionment calculations are available in Rodríguez et al. (2020a).

3. Results and discussion

Figure 1A shows the average dust distribution during our study and the main industrial areas of North Africa. Dust transport occurs primarily in the Saharan Air Layer, an elevated air stream located at altitudes 1–5 km off North Africa and < 3–4 km in the western North Atlantic(Prospero and Carlson, 1972; Tsamalis et al., 2013). Dust inputs to the ocean are estimated in 450 Tg/year and ~43% occur in the Atlantic(Huneeus et al., 2011; Jickells, 2005). Thus, this study was
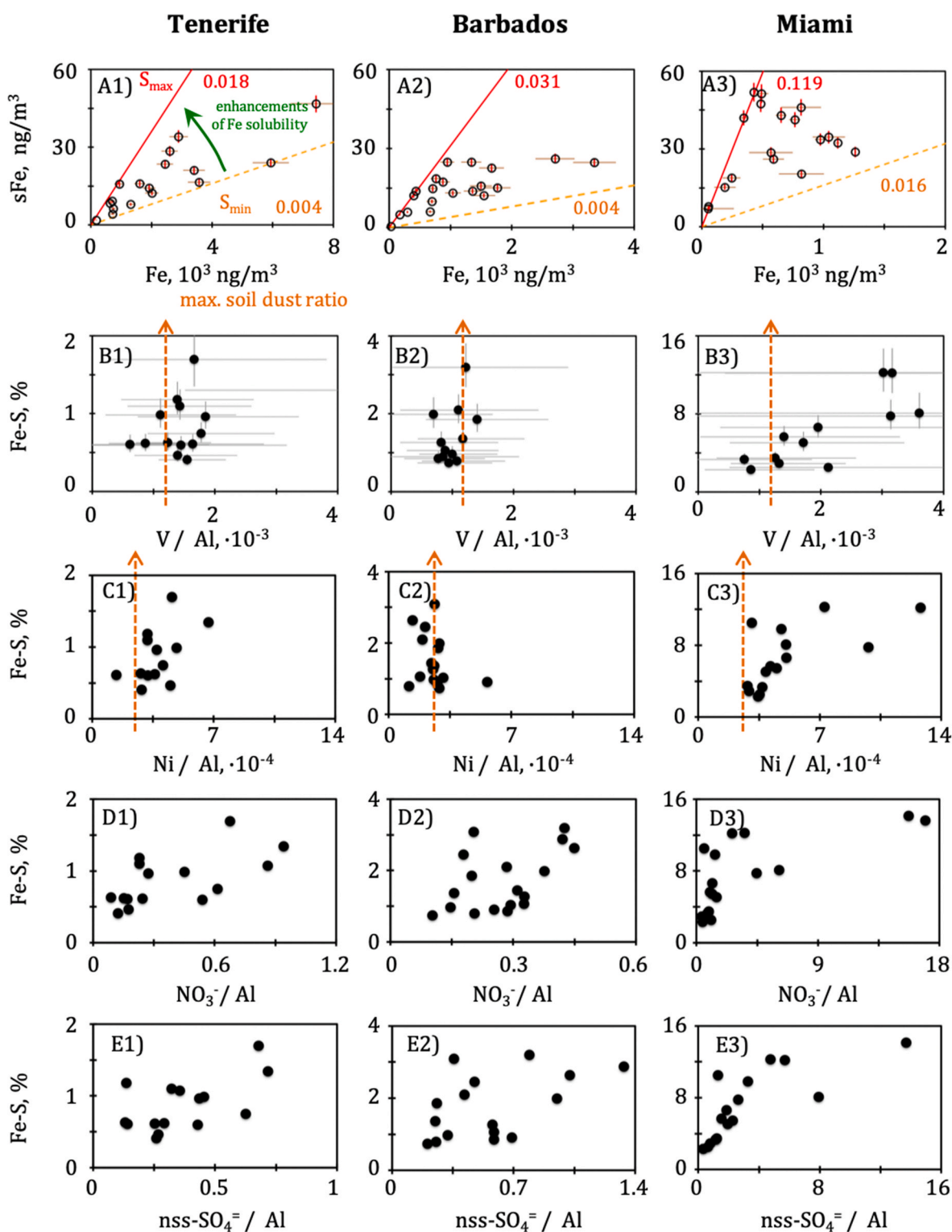
Fig. 4. A) sFe versus Fe. B-E) Fe–S versus the ratio of vanadium, nickel, nitrate and nss-sulphate to aluminium. A) The orange dashed and red lines (A1-A3) indicate the lines with minimum (S_{min}) and maximum (S_{max}) slopes comprising the data set. The vertical red and horizontal brown bars of each dot represent the uncertainty intervals of sFe and Fe, respectively. B) The vertical and horizontal grey bars of each dot represent the uncertainty intervals of Fe–S and the V/Al ratio, respectively. The vertical orange dashed line indicate the value of V/Al, $1.15 \cdot 10^{-3}$ (B1–B3), and Ni/Al, $2.5 \cdot 10^{-4}$ (C1–C3), above which increases in Fe–S are observed. (For interpretation of the references to colour in this figure legend, the reader is referred to the Web version of this article.)

designed to measure iron solubility in seawater, as an approach to mimic iron dissolution in the ocean resulted from dry deposition. The use of real seawater allows considering the potential role of the organic ligands present in the ocean, which complex Fe to keep it in solution in excess of its solubility (Hassler et al., 2011; Laglera and van den Berg, 2009).

Other approaches focus on mimicking in-cloud processing (e.g. sample extraction at pH 2 to 5 in deionized water) (Baker et al., 2016; Baker and Jickells, 2017; Buck et al., 2010; Meskhidze et al., 2016a). We will refer to soluble iron and iron solubility as sFe and Fe–S, respectively.

Table 1

Average (±1standard deviation) aerosol composition during the arrival of the dust-outbreak fronts (O1–O4) to Tenerife (T), Barbados (B) and Miami (M) in summer 2015. Impacts at Barbados and Miami occurring 3–6 days and 7–12 days later, respectively, after arrival at Tenerife and/or Cape Verde. O1 impact: 6–7 July (T), 15 July (B) and 17–18 July (M). O2 impact: 10-11-July (T), 17–18 July (B) and 20-21-July (M). O3 impact: 22-24-July (T), 26–27 July (B) and 1-3-August (M). O4 impact: 12-13-August (T) and 20–22 July (B). sFe_d: fraction of sFe due to dust. sFe_c: fraction of sFe due to HFO combustion. sFe_a: fraction of sFe due to atmospheric processing. sFe_c (and consequently) was estimated with two approaches: minimum ratio (min-R) and lower border line (LBL) methods. The contributions (%) of sFe_d, sFe_c and sFe_a to sFe is shown.

			Tenerife		Barbados		Miami	
			day: 0		day: + 3-6		day: + 7-12	
A)	dust	µg/m³	99.8 ± 48.1		53.2 ± 20.1		18.8 ± 5.7	
	Fe	µg/m³	3.3 ± 1.4		1.7 ± 1.2		0.8 ± 0.2	
	Al	µg/m³	6.9 ± 2.8		4.4 ± 1.6		1.8 ± 0.6	
B)	NO_3^-	µg/m³	1.3 ± 0.1		0.9 ± 0.3		1.6 ± 0.4	
	NH_4^+	µg/m³	0.4 ± 0.1		0.2 ± 0.1		0.3 ± 0.1	
	nss-SO_4^-	µg/m³	2.0 ± 0.7		1.7 ± 0.7		2.4 ± 0.4	
C)	Fe–S	%	0.69 ± 0.28		1.00 ± 0.27		4.71 ± 1.57	
D)	sFe	ng/m³	21.0 ± 5.8		19.6 ± 4.8		36.9 ± 7.3	
E) min-R	sFe_d	ng/m³	13.3 ± 5.6	(63%)	8.3 ± 3.4	(42%)	3.4 ± 1.0	(9%)
	sFe_c	ng/m³	1.9 ± 1.3	(9%)	1.7 ± 3.5	(9%)	9.6 ± 5.7	(26%)
	sFe_a	ng/m³	5.8 ± 1.2	(27%)	9.0 ± 0.7	(46%)	24.0 ± 0.7	(65%)
F) LBL	sFe_d	ng/m³	13.3 ± 5.6	(63%)	8.3 ± 3.4	(42%)	3.4 ± 1.0	(9%)
	sFe_c	ng/m³	2.4 ± 4.4	(11%)	2.9 ± 5.9	(15%)	2.5 ± 4.2	(7%)
	sFe_a	ng/m³	5.3 ± 3.7	(25%)	8.4 ± 3.0	(43%)	31.0 ± 2.2	(84%)

3.1. Transits of dust across the North Atlantic

Fig. 2 shows dust concentrations and AOD in Tenerife, in Barbados and in Miami. AOD at Cape Verde was also included (Fig. 2B). We tracked dust transits across the Atlantic with the MERRA-2 model; Fig. 3 shown an example on 23–31 July 2015. Measurements and model showed a good agreement (Figure S1-S2), a fact also observed in previous studies (Kramer et al., 2020).

Massive exports of dust occur in events of pulsating nature, at the rate of ~1 or 2 events/10 days, linked to east-to-west shifts of meteorological systems into North Africa (Cuevas et al., 2017; Rodríguez et al., 2020b). These dust outbreaks start with a dust-front expanding (South-North) along the African coast, across thousands of kilometres, e. g. from Cape Verde to Canary Islands (Fig. 3A). Then the outbreak propagates westward (Fig. 3B–E). The arrival of a dust-front to each measurement site resulted in increases in dust and AOD (Fig. 2). We detected four massive dust outbreaks; the peak-dust events associated with each dust-front is highlighted in Fig. 2 (outbreaks 1 to 4, O1–O4). Fig. 3 shows outbreak O3. Dust-fronts first impacted on Tenerife and/or Cape Verde, 3–6 days later in Barbados and 7–12 days later in Miami. Dust-fronts expand (South-North) along thousand of kilometres, consequently, a dusty air-parcel that impact Tenerife does not necessarily impacts Barbados and/or Miami. Dust impacting at a specific site could be linked to different dust source regions in North Africa. This is corroborated by the back-trajectories (Stein et al., 2015) associated with O1 to O4 at each site (Figure S3).

The arrival of the dust-fronts is associated with an increase in dust concentrations at each site, up to reach an average value, during the outbreaks O1–O4, of ~100, 53 and 19 µg/m³ in Tenerife, Barbados and Miami, respectively (Table 1A). After the dust-fronts passed, dust concentrations decreased, resulting in a dust background levels across the Atlantic (<20, <10 and < 8 µg/m³ at Tenerife, Barbados and Miami, respectively).

3.2. Iron solubility

At the three sites, iron showed a high linear relationship with aluminium and dust ($r^2 > 0.9$), with a slope (mass ratio, g/g) of Fe-to-dust within the range 0.034–0.039 and of Fe-to-Al 0.42–0.44 (Figure S4). These values are within the range of the typical Fe-to-Al ratio (0.4–0.5) and mean content of Fe in African dust (3–4%) (Rodríguez et al., 2020b; Pérez García-Pando et al., 2016; Scheuvens et al., 2013). This points that dust is the major source of iron at the three sites,

a fact observed previously (Ravelo-Pérez et al., 2016; Trapp et al., 2010a, 2010b).

Fig. 1B shows the plot of Fe–S versus Fe in Tenerife, Barbados and Miami. The inverse relationship observed in previous global studies (Sholkovitz et al., 2012), with low Fe–S (~0.4%) under high Fe concentrations and high Fe–S (~13%) under low Fe concentrations, is observed. There is a westward increase of Fe–S, with most of the values within the range 0.4–1.8% in Tenerife, 0.4–3.1% in Barbados and 1.0–12% in Miami. Previous studies also observed increases in Fe–S in dusty air, from 0.4% to 10%, after a few days of atmospheric transport (Ito and Feng, 2010; Luo and Gao, 2010; Meskhidze, 2005). Thus, we focused on identifying the sources and processes that contribute to such increases in Fe–S along the path of African dust outbreaks.

Fig. 4A1-4A3 shows the scatter plot of sFe versus Fe. At each site, the data set tends to be distributed between two linear boundaries, one with a minimum slope S_{min} and the other a maximum slope S_{max}. These represent the minimum and maximum iron solubilities, respectively. In Tenerife and Barbados, we found $S_{min} = 0.004$, which corresponds to a minimum Fe–S = 0.4% (orange dashed line in Fig. 4A1-4A2). This result is consistent with previous studies which found that the solubility of iron contained in desert dust aerosols is ~0.45% (Ravelo-Pérez et al., 2016; Sedwick et al., 2007; Shi et al., 2012; Theodosi et al., 2010), which is also the input value in many models (Ito, 2013; Ito et al., 2019; Ito and Feng, 2010; Johnson and Meskhidze, 2013; Wang et al., 2015). The data above this line (green arrow, Fig. 4A) of slope S_{min} indicates that sources other than dust provide sFe, increasing the Fe–S up to a maximum value represented by S_{max} (red line in Fig. 4A1-4A3). These additional inputs result in a maximum Fe–S = 1.8% in Tenerife (S_{max}; Fig. 4A1) and = 3.1% in Barbados (S_{max}; Fig. 4A2). At Miami (Fig. 4A3), the slopes S_{min} (=0.016) and S_{max} (=0.119) are significantly higher than in Tenerife and Barbados, a result that indicates that in addition to dust, there are important additional contributions to sFe.

We investigated the potential contributions to sFe due to HFO combustion and due to iron dissolution by acid pollutants. Aluminium was used as dust tracer, vanadium and nickel as tracers of HFO combustion emissions (Baker et al., 2016; Baker and Jickells, 2017; Becagli et al., 2012; Sedwick et al., 2007) and nitrate, non sea salt (nss) sulphate and ammonium as tracers of (nitric and sulphuric) acids (Baker et al., 2016; Sholkovitz et al., 2009). HFO is used for shipping and for power generation and its combustion is associated with the emissions of fly ashes and (nitric and sulphuric) acids precursors (SO_2 and NO_x; Becagli et al., 2012, and references therein). Saharan dust over the Atlantic is regularly mixed with these pollutants (Baker and Jickells, 2017;
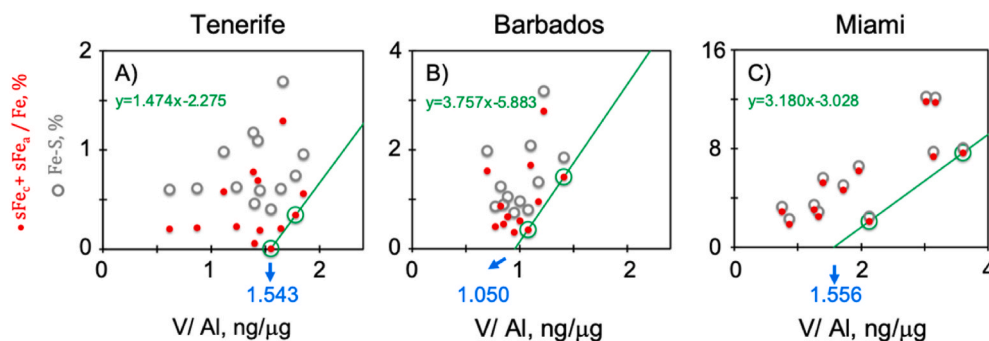
Fig. 5. Ratio ($sFe_d + sFe_c + sFe_a$) to Fe (grey dots). Ratio of ($sFe_c + sFe_a$) to Fe (green dots). In green colour are highlighted the two points (circles) representative of the lower border of the data set, the resulting fitting equation ($y = A·x + B$) and line. Blue numbers indicate the point at which the fitting line cross X-axis. (For interpretation of the references to colour in this figure legend, the reader is referred to the Web version of this article.)

Rodríguez et al., 2011, 2020b; Trapp et al., 2010a), linked to emissions in Europe (Kallos et al., 1998), ships in the Mediterranean (Becagli et al., 2012; Kallos et al., 2007) and the North African industry (Fig. 1A; Rodríguez et al., 2011).

3.3. Traces of heavy fuel oil combustion

Fe-S tends to increase when the ratios V/Al and Ni/Al increase above the thresholds V/Al ~$1.15·10^{-3}$ and Ni/Al ~$2.5·10^{-4}$ (Fig. 4B1-4C1). These thresholds are very close to those representative of the V and Ni ratios to Al in Saharan dust (Eglinton et al., 2002; Sholkovitz et al., 2009). Data with a V/Al and Ni/Al ratios higher than those dust-thresholds indicate an excess of V and Ni in the aerosols, with respect to dust, likely linked to the presence of traces pollutants linked to HFO combustion (Trapp et al., 2010a) which usually containing soluble ferric sulphate and nanocrystals of magnetite (Fu et al., 2012; Schroth et al., 2009).

By using equations 3, 4 and 5, we estimate that ~23, 15 and 28% of V measured at Tenerife, Barbados and Miami during this experiment is due to HFO combustion, respectively, i.e. dust is still the dominant source of V during dust outbreaks. The V/Al ratios we observed in dust outbreaks (Fig. 4B1-4B3) are close to those reported previously ($<2·10^{-3}$), but lower than those found in the polluted marine atmosphere (V/Al: 10–80 ·10^{-3}; (Sedwick et al., 2007; Wozniak et al., 2013, 2015). Similar results are found for the Ni/Al ratios: 2–14·10^{-4} in Saharan dusty air (Fig. 4B1-4B3) and 150–300·10^{-4} in the polluted marine atmosphere (Wozniak et al., 2013).

3.4. Traces of acid processing

Fe-S also increases when the ratios of nitrate (Fig. 4D1-4D3), nss-sulphate (Fig. 4E1-4E3) and ammonium to aluminium increased. The formation of these salts involves nitric and sulphuric acids and potential acidity during some stages after the emissions of their precursors (Chen and Grassian, 2013; Li et al., 2017; Longo et al., 2016). The reaction of dust with acids contributes to Fe dissolution, with an efficiency modulated by minerals with buffering capacity (Ito and Feng, 2010). Organic acids, linked to water-soluble organic matter mixed with dust (Zamora et al., 2011), may also contribute to sFe (Wozniak et al., 2013). Carboxylic acids may complex Fe and maintain it with an enhanced solubility (Hawkins et al., 2010; Okochi and Brimblecombe, 2002).

Although previous studies found that other sources (e.g. biomass burning or coal power-plants (Kanakidou et al., 2018; Mahowald et al., 2018) may also contribute to sFe), we did not identified their involvement during our study. This result is not surprising in the summer when biomass burning is at a minimum in North Africa.

3.5. Source apportionment of soluble iron

We used two approaches, the minimum ratio method (Na et al., 2004; Turpin and Huntzicker, 1995) and lower border line (Kulmala et al., 2016; Reche et al., 2011; Rodríguez and Cuevas, 2007), and the above-described relationships (Fig. 4) for apportioning sFe between the contributions of dust (sFe_d), HFO combustion (sFe_c) and atmospheric processing (sFe_a), by equations (6)–(9):

$$sFe = sFe_d + sFe_c + sFe_a \tag{6a}$$

$$sFe_d = S_{min}·Fe \tag{7}$$

$$100\frac{sFe_c}{Fe} = Z_{min}\frac{V}{Al} + C_{min} \tag{8a}$$

$$sFe_c = \begin{cases} 0, & \left(\frac{V}{Al}\right) \leq \left(\frac{V}{Al}\right)_d \\ \frac{Fe}{100}\left[Z_{min}\frac{V}{Al} + C_{min}\right], & \left(\frac{V}{Al}\right) > \left(\frac{V}{Al}\right)_d \end{cases} \tag{8b}$$

$$sFe_a = sFe - (sFe_d + sFe_c) \tag{6b}$$

The contribution of sFe_d was determined using S_{min} (= 0.004), representative of the solubility of Fe in dust (0.4%) observed in this (Fig. 4A1 and Fig. 4A2) and in previous studies (Ravelo-Pérez et al., 2016; Schroth et al., 2009; Sedwick et al., 2007; Theodosi et al., 2010). Two approaches were used for determining sFe_c (equation (8)), based on the minimum ratio and the lower border line. This sFe_c component only contributes to sFe when the V/Al ratio is higher than a $(V/Al)_d$ threshold. Finally, sFe_a was calculated with equation (6b).

In the minimum ratio (min-R) approach to determine sFe_c (equations (8a)-(8b))), $C_{min} = 0$ and Z_{min} is the minimum value found in the 100· ($sFe_c + sFe_a$/Fe)/(V/Al) ratios in the collection of samples at each site, where $sFe_c + sFe_a$ is the difference between sFe and sFe_d (equation (6a)). We found Z_{min} values (dimensionless mass ratio) equal to 44.5 in Tenerife, 355.7 in Barbados and 988.0 in Miami. The low Z_{min} values in Tenerife are due to the low Fe–S at this site. A threshold value $(V/Al)_d$ = $1.15·10^{-3}$ was used (mass ratio), as proxy of the maximum amount of vanadium in Saharan dust (Eglinton et al., 2002).

The lower border line (LBL) approach to determine sFe_c (Rodríguez and Cuevas, 2007), Z_{min} and C_{min} are calculated by regression analysis, as the fitting equation of the lower border line of the plot of 100·($sFe_c + sFe_a$)/Fe versus V/Al, where $sFe_c + sFe_a$ is determined as the difference between sFe and sFe_d (equation (6a)). This plot is shown in Fig. 5 (red dots), where, in green colour, are highlighted the two points (circles) representative of the lower border of the data set and the resulting regression line and equation. This (green) line represents the minimum increase of iron solubility associated with the increases of vanadium with respect to aluminium, and it is considered a proxy of the
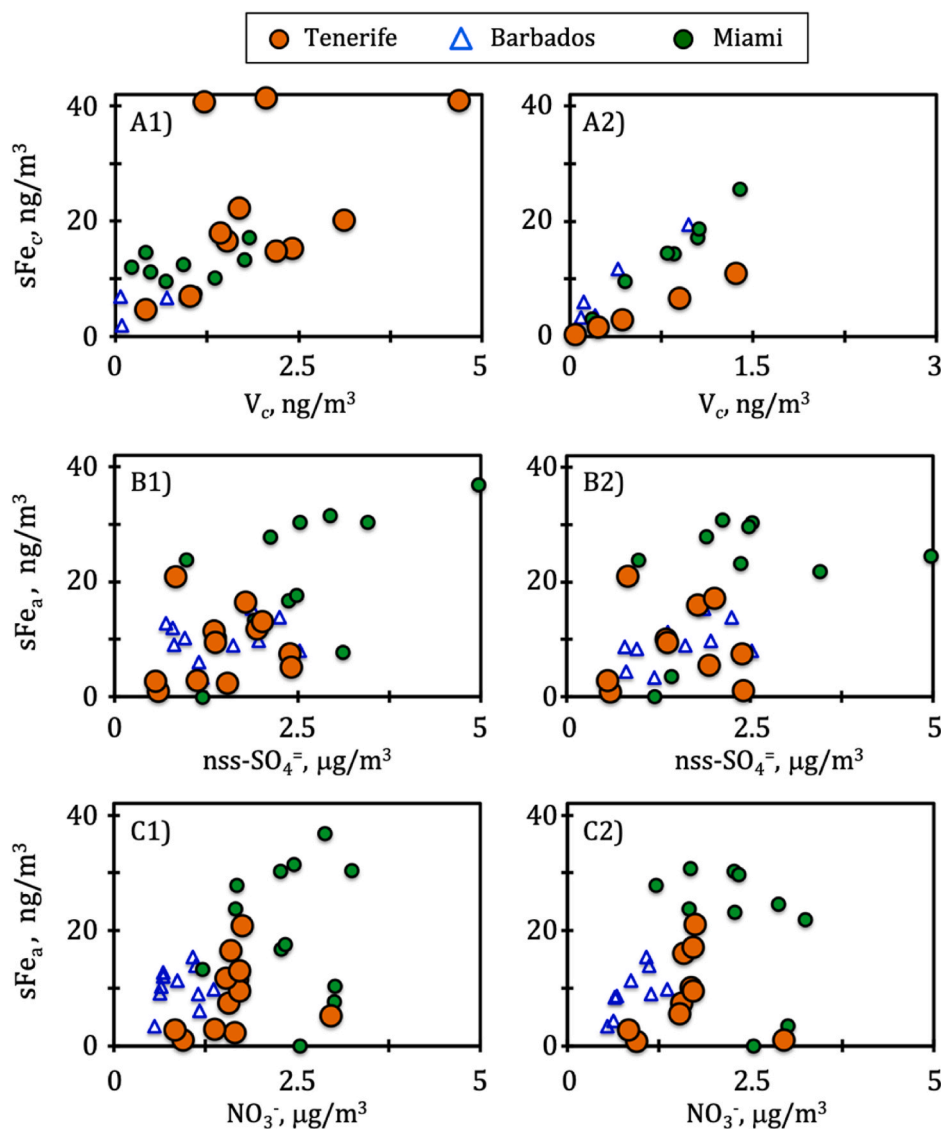
Fig. 6. A) Soluble iron due to HFO combustion (sFe$_c$) versus vanadium due to HFO combustion (V$_c$). A1) data of Tenerife are multiplied by 10, scale factor. B-D) Soluble iron due to atmospheric processing sFe$_a$ versus nitrate, none sea salt sulphate and ammonium. Plots include all data (not only dust-front impact events) collected in summer 2015. Results obtained with the minimum ratio and lower border line methods are shown in columns (A1-C1) and (A2-C2), respectively.

contribution of HFO combustion to soluble iron due to emissions of fly ashes containing soluble ferric sulphate and nanocrystals of magnetite (Fu et al., 2012; Schroth et al., 2009). In this method the (V/Al)$_d$ threshold is determined as:

$$\left(\frac{V}{Al}\right)_d = -\left(\frac{C_{min}}{Z_{min}}\right) \tag{9}$$

The regression equation and (V/Al)$_d$ thresholds obtained with this method are shown in green and blue, respectively, in Fig. 5. The (V/Al)$_d$ thresholds (ng/μg) above wich we observe an increase in iron solubility is 1.543 in Tenerife, 1.050 in Barbados and 1.556 in Miami. This experimental procedure to determine (V/Al)$_d$ allow to take into account the potential variability in the V/Al ratios in dust and in the relationship between sFe$_c$ and V$_c$ in HFO combustion emissions.

We applied these two (R-min and LBL) methods (equations (6)–(9)) to the collected data set. The correlation of sFe$_c$ with V$_c$ (Fig. 6A) and the increasing trend of sFe$_a$ with sulphate and nitrate (Fig. 6B–C) support the consistency of the approaches.

We first focused on the peak dust events due to the impact of the dust-fronts at each site (Table 1), described previously. The overall data

analysis indicates that during the Atlantic transit of the dust Saharan outbreaks, dust contributions (sFe$_d$) to sFe decrease from 63% (Tenerife) down to 9% (Miami), whereas sFe$_a$ + sFe$_c$ (joined effects of air pollutants) accounts for 35% (Tenerife) to 91% (Miami) of sFe (Tables 1E and 1F).

During the impact of the dust-outbreak fronts, Fe concentrations decreased across Tenerife, Barbados and Miami, 3.3, 1.7 and 0.8 μg/m³, whereas Fe–S increased: 0.69%, 1.00% and 4.71% (Table 1C), respectively. This westward increase of Fe–S is associated with (i) a decrease of sFe$_d$, linked to (size depended) dust deposition across the Atlantic (13.3–3.4 ng/m³; Table 1E–1F), and (ii) an increase in the contribution of atmospheric processing (sFe$_a$ 5–6 to 24–31 ng/m³; Table 1E-1F), consistent with previous studies that found increasing amounts of soluble Fe(II)-sulphate on Saharan dust because of the effects of acids, even after 10 days of atmospheric transport (Longo et al., 2016). In Tenerife, sFe$_a$ accounts for ~25–27% of sFe (Tables 1E-1F), which suggests that atmospheric processing of dust may already have occurred over North Africa (Ravelo-Pérez et al., 2016). Regional emissions of acid precursors in the Caribbean (Zamora et al., 2013) and in-cloud processing (Buck et al., 2010; Shi et al., 2009) may account for the observed increase of sFe$_a$ from Barbados to Miami. We observed that sFe$_c$ concentrations are
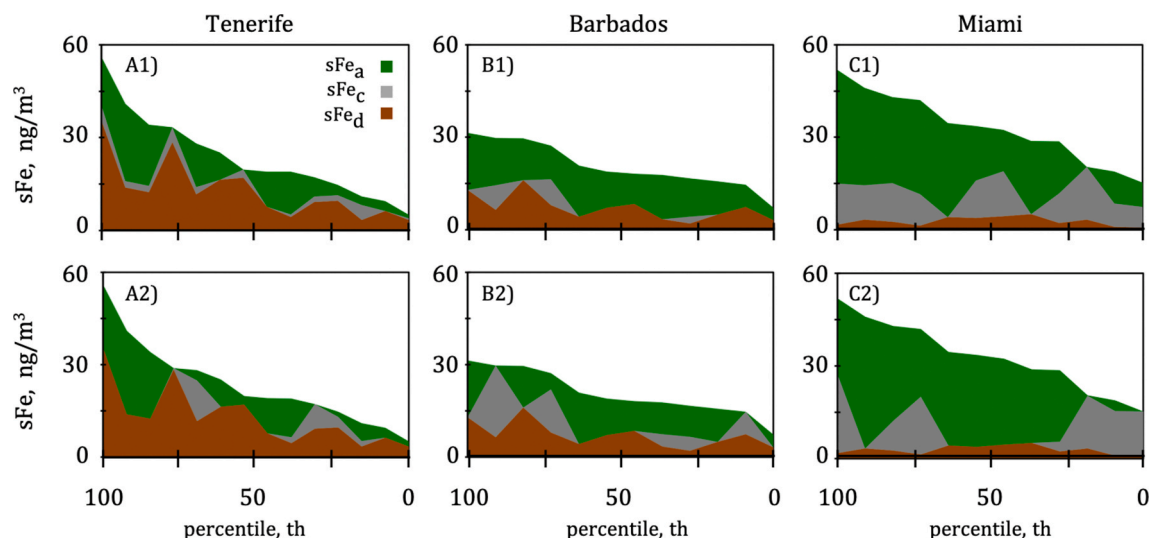
Fig. 7. Concentrations of soluble iron (sFe) classified from highest to lowest values. The contributions of dust (brown), HFO combustion (grey) and atmospheric processing (green) are highlighted in brown, grey and green colour, respectively. Two approaches were used: A1-C1 is based on the minimum ratio method, whereas A2-C2 is based on the lower border line method. Plots include all data (not only dust front events) generated in summer 2015. (For interpretation of the references to colour in this figure legend, the reader is referred to the Web version of this article.)

mostly ≤ 5 ng/m^3 (Table 1D), which are lower than those that we estimate for the polluted marine atmosphere, sFe$_c$ = 10–200 ng/m^3 (based on equations (8b)-(8c) and previous data of Sedwick et al., 2007 and Wozniak et al., 2013, 2015). This rather low contribution of sFe$_c$ is due to the fact that the V/Al ratios are not much higher than the (V/Al)$_d$ thresholds in dust.

Fig. 7 shows all data of sFe concentration at each site, including the contributions of sFe$_d$, sFe$_c$ and sFe$_a$, generated in this study, classified from the highest to the lowest sFe value. This plot include all available data, i.e. peak dust events due to the impact of the dust-fronts at each and other days. In Tenerife, increases in sFe are linked to increases in the contributions of sFe$_d$ and sFe$_a$. In Barbados, the contribution of sFe$_a$ is somewhat higher than in Tenerife, whereas in Miami the contribution of sFe$_a$ is dominant. For sFe concentrations within the range 20–80th percentiles, sFe$_d$ and sFe$_a$ + sFe$_c$ accounts for 57% and 43% (37 + 8% and 30 + 13%, based on min-R and LBL, respectively) in Tenerife, 33% and 67% (61 + 6% and 53 + 14%) in Barbados and 10% and 90% (61 + 29% and 71 + 18%) in Miami, respectively. These results support the idea that the mixing of dust with acid pollutants is an important source of soluble iron as Saharan-dust outbreaks traverse the Atlantic.

CRediT authorship contribution statement

Sergio Rodríguez: Conceptualization, Data curation, Formal analysis, Funding acquisition, Investigation, Methodology, Project administration, Resources, Supervision, Writing - original draft, Writing - review & editing. **Joseph M. Prospero:** Conceptualization, Data curation, Investigation, Methodology, Resources, Supervision, Writing - original draft, Writing - review & editing. **Jessica López-Darias:** Data curation, Formal analysis, Writing - review & editing. **María-Isabel García-Alvarez:** Data curation, Formal analysis, Writing - review & editing. **Paquita Zuidema:** Data curation, Methodology, Resources, Writing - review & editing. **Silvia Nava:** Data curation, Writing - review & editing. **Franco Lucarelli:** Conceptualization, Data curation, Methodology, Writing - review & editing. **Cassandra J. Gaston:** Writing - review & editing. **Luis Galindo:** Data curation, Methodology, Writing - review & editing. **Elisa Sosa:** Data curation, Writing - review & editing.

Declaration of competing interest

The authors declare that they have no known competing financial interests or personal relationships that could have appeared to influence the work reported in this paper.

EUROPEAN UNION
European Regional Development Fund

Appendix A. Supplementary data

Supplementary data to this article can be found online at https://doi.org/10.1016/j.atmosenv.2020.118092.

References

Aguilar-Islas, A.M., Wu, J., Rember, R., Johansen, A.M., Shank, L.M., 2010. Dissolution of aerosol-derived iron in seawater: leach solution chemistry, aerosol type, and colloidal iron fraction. Mar. Chem. 120 (1–4), 25–33. https://doi.org/10.1016/j.marchem.2009.01.011.

Ahlgren, N.A., Noble, A., Patton, A.P., Roache-Johnson, K., Jackson, L., Robinson, D., McKay, C., Moore, L.R., Saito, M.A., Rocap, G., 2014. The unique trace metal and mixed layer conditions of the Costa Rica upwelling dome support a distinct and

dense community of Synechococcus. Limnol. Oceanogr. 59 (6), 2166–2184. https://doi.org/10.4319/lo.2014.59.6.2166.

Ault, A.P., Gaston, C.J., Wang, Y., Dominguez, G., Thiemens, M.H., Prather, K.A., 2010. Characterization of the single particle mixing state of individual ship plume events measured at the port of Los Angeles. Environ. Sci. Technol. 44 (6), 1954–1961. https://doi.org/10.1021/es902985h.

de Baar, H.J.W., 2005. Synthesis of iron fertilization experiments: from the iron age in the age of enlightenment. J. Geophys. Res. 110 (C9), C09S16. https://doi.org/10.1029/2004JC002601.

Baker, A.R., Jickells, T.D., 2006. Mineral particle size as a control on aerosol iron solubility. Geophys. Res. Lett. 33 (17), L17608. https://doi.org/10.1029/2006GL026557.

Baker, A.R., Jickells, T.D., 2017. Atmospheric deposition of soluble trace elements along the Atlantic Meridional Transect (AMT). Prog. Oceanogr. 158, 41–51. https://doi.org/10.1016/j.pocean.2016.10.002.

Baker, A.R., Landing, W.M., Bucciarelli, E., Cheize, M., Fietz, S., Hayes, C.T., Kadko, D., Morton, P.L., Rogan, N., Sarthou, G., Shelley, R.U., Shi, Z., Shiller, A., van Hulten, M.M.P., 2016. Trace element and isotope deposition across the air–sea interface: progress and research needs. Philos. Trans. R. Soc. A Math. Phys. Eng. Sci. 374 (2081), 20160190. https://doi.org/10.1098/rsta.2016.0190.

Barkley, A.E., Prospero, J.M., Mahowald, N., Hamilton, D.S., Popendorf, K.J., Oehlert, A.M., Pourmand, A., Gatineau, A., Panechou-Pulcherie, K., Blackwelder, P., Gaston, C.J., 2019. African biomass burning is a substantial source of phosphorus deposition to the Amazon, Tropical Atlantic Ocean, and Southern Ocean. Proc. Natl. Acad. Sci. Unit. States Am. 116 (33), 16216–16221. https://doi.org/10.1073/pnas.1906091116.

Becagli, S., Sferlazzo, D.M., Pace, G., di Sarra, A., Bommarito, C., Calzolai, G., Ghedini, C., Lucarelli, F., Meloni, D., Monteleone, F., Severi, M., Traversi, R., Udisti, R., 2012. Evidence for heavy fuel oil combustion aerosols from chemical analyses at the island of Lampedusa: a possible large role of ships emissions in the Mediterranean. Atmos. Chem. Phys. 12 (7), 3479–3492. https://doi.org/10.5194/acp-12-3479-2012.

Boyd, P.W., Jickells, T., Law, C.S., Blain, S., Boyle, E.A., Buesseler, K.O., Coale, K.H., Cullen, J.J., de Baar, H.J.W., Follows, M., Harvey, M., Lancelot, C., Levasseur, M., Owens, N.P.J., Pollard, R., Rivkin, R.B., Sarmiento, J., Schoemann, V., Smetacek, V., Takeda, S., Tsuda, A., Turner, S., Watson, A.J., 2007. Mesoscale iron enrichment experiments 1993-2005: synthesis and future directions (80-.). Science 315 (5812), 612–617. https://doi.org/10.1126/science.1131669.

Boye, M., Nishioka, J., Croot, P., Laan, P., Timmermans, K.R., Strass, V.H., Takeda, S., de Baar, H.J.W., 2010. Significant portion of dissolved organic Fe complexes in fact is Fe colloids. Mar. Chem. 122 (1–4), 20–27. https://doi.org/10.1016/j.marchem.2010.09.001.

Browning, T.J., Bouman, H.A., Henderson, G.M., Mather, T.A., Pyle, D.M., Schlosser, C., Woodward, E.M.S., Moore, C.M., 2014. Strong responses of Southern Ocean phytoplankton communities to volcanic ash. Geophys. Res. Lett. 41 (8), 2851–2857. https://doi.org/10.1002/2014GL059364.

Buck, C.S., Landing, W.M., Resing, J.A., Lebon, G.T., 2006. Aerosol iron and aluminum solubility in the northwest Pacific Ocean: results from the 2002 IOC cruise. G-cubed 7 (4). https://doi.org/10.1029/2005GC000977 n/a-n/a.

Buck, C.S., Landing, W.M., Resing, J.A., Measures, C.I., 2010. The solubility and deposition of aerosol Fe and other trace elements in the North Atlantic Ocean: observations from the A16N CLIVAR/CO2 repeat hydrography section. Mar. Chem. 120 (1–4), 57–70. https://doi.org/10.1016/j.marchem.2008.08.003.

Buck, K.N., Sohst, B., Sedwick, P.N., 2015. The organic complexation of dissolved iron along the U.S. GEOTRACES (GA03) North Atlantic Section. Deep Sea Res. Part II Top. Stud. Oceanogr. 116, 152–165. https://doi.org/10.1016/j.dsr2.2014.11.016.

Calzolai, G., Lucarelli, F., Chiari, M., Nava, S., Giannoni, M., Carraresi, L., Prati, P., Vecchi, R., 2015. Improvements in PIXE analysis of hourly particulate matter samples. Nucl. Instrum. Methods Phys. Res. Sect. B Beam Interact. Mater. Atoms 363, 99–104. https://doi.org/10.1016/j.nimb.2015.08.022.

Chapman, R.L., 2013. Algae: the world's most important "plants"—an introduction. Mitig. Adapt. Strategies Glob. Change 18 (1), 5–12. https://doi.org/10.1007/s11027-010-9255-9.

Chen, H., Grassian, V.H., 2013. Iron dissolution of dust source materials during simulated acidic processing: the effect of sulfuric, acetic, and oxalic acids. Environ. Sci. Technol. https://doi.org/10.1021/es401285s, 130829091001000.

Chen, H., Laskin, A., Baltrusaitis, J., Gorski, C.A., Scherer, M.M., Grassian, V.H., 2012. Coal fly ash as a source of iron in atmospheric dust. Environ. Sci. Technol. 46 (4), 2112–2120. https://doi.org/10.1021/es204102f.

Cuevas, E., Gómez-Peláez, A.J., Rodríguez, S., Terradellas, E., Basart, S., García, R.D., García, O.E., Alonso-Pérez, S., 2017. The pulsating nature of large-scale Saharan dust transport as a result of interplays between mid-latitude Rossby waves and the North African Dipole Intensity. Atmos. Environ. 167, 586–602. https://doi.org/10.1016/j.atmosenv.2017.08.059.

Duce, R., Galloway, J., Liss, P., 2009. The impacts of atmospheric deposition to the ocean on marine ecosystems and climate. WMO Bull (58), 61–66.

Duce, R.A., LaRoche, J., Altieri, K., Arrigo, K.R., Baker, A.R., Capone, D.G., Cornell, S., Dentener, F., Galloway, J., Ganeshram, R.S., Geider, R.J., Jickells, T., Kuypers, M.M., Langlois, R., Liss, P.S., Liu, S.M., Middelburg, J.J., Moore, C.M., Nickovic, S., Oschlies, A., Pedersen, T., Prospero, J., Schlitzer, R., Seitzinger, S., Sorensen, L.L., Uematsu, M., Ulloa, O., Voss, M., Ward, B., Zamora, L., 2008. Impacts of atmospheric anthropogenic nitrogen on the open ocean. Science (80-.) 320 (5878), 893–897. https://doi.org/10.1126/science.1150369.

Eglinton, T.I., Eglinton, G., Dupont, L., Sholkovitz, E.R., Montluçon, D., Reddy, C.M., 2002. Composition, age, and provenance of organic matter in NW African dust over the Atlantic Ocean. G-cubed 3 (8), 1–27. https://doi.org/10.1029/2001GC000269.

Falkowski, P.G., 1998. Biogeochemical controls and feedbacks on ocean primary production. Science (80-.) 281 (5374), 200–206. https://doi.org/10.1126/science.281.5374.200.

Fitzsimmons, J.N., Carrasco, G.G., Wu, J., Roshan, S., Hatta, M., Measures, C.I., Conway, T.M., John, S.G., Boyle, E.A., 2015. Partitioning of dissolved iron and iron isotopes into soluble and colloidal phases along the GA03 GEOTRACES North Atlantic Transect. Deep Sea Res. Part II Top. Stud. Oceanogr. 116, 130–151. https://doi.org/10.1016/j.dsr2.2014.11.014.

Fu, H., Cwiertny, D.M., Carmichael, G.R., Scherer, M.M., Grassian, V.H., 2010. Photoreductive dissolution of Fe-containing mineral dust particles in acidic media. J. Geophys. Res. 115 (D11), D11304. https://doi.org/10.1029/2009JD012702.

Fu, H., Lin, J., Shang, G., Dong, W., Grassian, V.H., Carmichael, G.R., Li, Y., Chen, J., 2012. Solubility of iron from combustion source particles in acidic media linked to iron speciation. Environ. Sci. Technol. 46 (20), 11119–11127. https://doi.org/10.1021/es302558m.

Gaston, C.J., 2020. Re-examining dust chemical aging and its impacts on Earth's climate. Acc. Chem. Res. https://doi.org/10.1021/acs.accounts.0c00102.

Gelaro, R., McCarty, W., Suárez, M.J., Todling, R., Molod, A., Takacs, L., Randles, C.A., Darmenov, A., Bosilovich, M.G., Reichle, R., Wargan, K., Coy, L., Cullather, R., Draper, C., Akella, S., Buchard, V., Conaty, A., da Silva, A.M., Gu, W., Kim, G.-K., Koster, R., Lucchesi, R., Merkova, D., Nielsen, J.E., Partyka, G., Pawson, S., Putman, W., Rienecker, M., Schubert, S.D., Sienkiewicz, M., Zhao, B., 2017. The Modern-era retrospective analysis for research and applications, version 2 (MERRA-2). J. Clim. 30 (14), 5419–5454. https://doi.org/10.1175/JCLI-D-16-0758.1.

Hassler, C.S., Schoemann, V., Nichols, C.M., Butler, E.C.V., Boyd, P.W., 2011. Saccharides enhance iron bioavailability to Southern Ocean phytoplankton. Proc. Natl. Acad. Sci. Unit. States Am. 108 (3), 1076–1081. https://doi.org/10.1073/pnas.1010963108.

Hawkins, L.N., Russell, L.M., Covert, D.S., Quinn, P.K., Bates, T.S., 2010. Carboxylic acids, sulfates, and organosulfates in processed continental organic aerosol over the southeast Pacific Ocean during VOCALS-REx 2008. J. Geophys. Res. 115 (D13), D13201. https://doi.org/10.1029/2009JD013276.

Hettiarachchi, E., Rubasinghege, G., 2020. Mechanistic study on iron solubility in atmospheric mineral dust aerosol: roles of titanium, dissolved oxygen, and solar flux in solutions containing different acid anions. ACS Earth Sp. Chem. 4 (1), 101–111. https://doi.org/10.1021/acsearthspacechem.9b00280.

Huneeus, N., Schulz, M., Balkanski, Y., Griesfeller, J., Prospero, J., Kinne, S., Bauer, S., Boucher, O., Chin, M., Dentener, F., Diehl, T., Easter, R., Fillmore, D., Ghan, S., Ginoux, P., Grini, A., Horowitz, L., Koch, D., Krol, M.C., Landing, W., Liu, X., Mahowald, N., Miller, R., Morcrette, J.-J., Myhre, G., Penner, J., Perlwitz, J., Stier, P., Takemura, T., Zender, C.S., 2011. Global dust model intercomparison in AeroCom phase I. Atmos. Chem. Phys. 11 (15), 7781–7816. https://doi.org/10.5194/acp-11-7781-2011.

Ingall, E., Feng, Y., Longo, A., Lai, B., Shelley, R., Landing, W., Morton, P., Nenes, A., Mihalopoulos, N., Violaki, K., Gao, Y., Sahai, S., Castorina, E., 2018. Enhanced iron solubility at low pH in global aerosols, atmosphere (basel), 9 (5), 201. https://doi.org/10.3390/atmos9050201.

Ito, A., 2013. Global modeling study of potentially bioavailable iron input from shipboard aerosol sources to the ocean. Global Biogeochem. Cycles 27 (1), 1–10. https://doi.org/10.1029/2012GB004378.

Ito, A., 2015. Atmospheric processing of combustion aerosols as a source of bioavailable iron. Environ. Sci. Technol. Lett. 2 (3), 70–75. https://doi.org/10.1021/acs.estlett.5b00007.

Ito, A., Feng, Y., 2010. Role of dust alkalinity in acid mobilization of iron. Atmos. Chem. Phys. 10 (19), 9237–9250. https://doi.org/10.5194/acp-10-9237-2010.

Ito, A., Shi, Z., 2016. Delivery of anthropogenic bioavailable iron from mineral dust and combustion aerosols to the ocean. Atmos. Chem. Phys. 16 (1), 85–99. https://doi.org/10.5194/acp-16-85-2016.

Ito, A., Xu, L., 2014. Response of acid mobilization of iron-containing mineral dust to improvement of air quality projected in the future. Atmos. Chem. Phys. 14 (7), 3441–3459. https://doi.org/10.5194/acp-14-3441-2014.

Ito, A., Myriokefalitakis, S., Kanakidou, M., Mahowald, N.M., Scanza, R.A., Hamilton, D.S., Baker, A.R., Jickells, T., Sarin, M., Bikkina, S., Gao, Y., Shelley, R.U., Buck, C.S., Landing, W.M., Bowie, A.R., Perron, M.M.G., Guieu, C., Meskhidze, N., Johnson, M.S., Feng, Y., Kok, J.F., Nenes, A., Duce, R.A., 2019. Pyrogenic iron: the missing link to high iron solubility in aerosols. Sci. Adv. 5 (5), eaau7671. https://doi.org/10.1126/sciadv.aau7671.

Ito, T., Nenes, A., Johnson, M.S., Meskhidze, N., Deutsch, C., 2016. Acceleration of oxygen decline in the tropical Pacific over the past decades by aerosol pollutants. Nat. Geosci. 9 (6), 443–447. https://doi.org/10.1038/ngeo2717.

Jickells, T., Boyd, P., Hunter, K.A., 2014. Biogeochemical impacts of dust on the global carbon cycle. Mineral Dust. Springer Netherlands, Dordrecht., pp. 359–384

Jickells, T.D., 2005. Global iron connections between desert dust, ocean biogeochemistry, and climate, 80- Science 308 (5718), 67–71. https://doi.org/10.1126/science.1105959.

Johnson, M.S., Meskhidze, N., 2013. Atmospheric dissolved iron deposition to the global oceans: effects of oxalate-promoted Fe dissolution, photochemical redox cycling, and dust mineralogy. Geosci. Model Dev. (GMD) 6 (4), 1137–1155. https://doi.org/10.5194/gmd-6-1137-2013.

Jordi, A., Basterretxea, G., Tovar-Sanchez, A., Alastuey, A., Querol, X., 2012. Copper aerosols inhibit phytoplankton growth in the Mediterranean Sea. Proc. Natl. Acad. Sci. Unit. States Am. 109 (52), 21246–21249. https://doi.org/10.1073/pnas.1207567110.

Journet, E., Desboeufs, K.V., Caquineau, S., Colin, J.-L., 2008. Mineralogy as a critical factor of dust iron solubility. Geophys. Res. Lett. 35 (7) https://doi.org/10.1029/2007GL031589 n/a-n/a.

Kallos, G., Kotroni, V., Lagouvardos, K., Papadopoulos, A., 1998. On the Long-Range transport of air pollutants from Europe to Africa. Geophys. Res. Lett. 25 (5), 619–622. https://doi.org/10.1029/97GL03317.

Kallos, G., Astitha, M., Katsafados, P., Spyrou, C., 2007. Long-range transport of anthropogenically and naturally produced particulate matter in the Mediterranean and North Atlantic: current state of knowledge. J. Appl. Meteorol. Climatol. 46 (8), 1230–1251. https://doi.org/10.1175/JAM2530.1.

Kanakidou, M., Myriokefalitakis, S., Tsigaridis, K., 2018. Aerosols in atmospheric chemistry and biogeochemical cycles of nutrients. Environ. Res. Lett. 13 (6), 063004 https://doi.org/10.1088/1748-9326/aabcdb.

Kramer, S.J., Alvarez, C., Barkley, A.E., Colarco, P.R., Custals, L., Delgadillo, R., Gaston, C.J., Govindaraju, R., Zuidema, P., 2020. Apparent dust size discrepancy in aerosol reanalysis in north African dust after long-range transport. Atmos. Chem. Phys. 20 (16), 10047–10062. https://doi.org/10.5194/acp-20-10047-2020.

Krishnamurthy, A., Moore, J.K., Mahowald, N., Luo, C., Zender, C.S., 2010. Impacts of atmospheric nutrient inputs on marine biogeochemistry. J. Geophys. Res. 115 (G1), G01006. https://doi.org/10.1029/2009JG001115.

Kulmala, M., Luoma, K., Virkkula, A., Petäjä, T., Paasonen, P., Kerminen, V.M., Nie, W., Qi, X., Shen, Y., Chi, X., Ding, A., 2016. On the mode-segregated aerosol particle number concentration load: contributions of primary and secondary particles in Hyytiälä and Nanjing. Boreal Environ. Res. 21 (3–4), 319–331.

Laglera, L.M., van den Berg, C.M.G., 2009. Evidence for geochemical control of iron by humic substances in seawater. Limnol. Oceanogr. 54 (2), 610–619. https://doi.org/10.4319/lo.2009.54.2.0610.

Li, W., Xu, L., Liu, X., Zhang, J., Lin, Y., Yao, X., Gao, H., Zhang, D., Chen, J., Wang, W., Harrison, R.M., Zhang, X., Shao, L., Fu, P., Nenes, A., Shi, Z., 2017. Air pollution–aerosol interactions produce more bioavailable iron for ocean ecosystems. Sci. Adv. 3 (3), 1–7. https://doi.org/10.1126/sciadv.1601749.

Longo, A.F., Feng, Y., Lai, B., Landing, W.M., Shelley, R.U., Nenes, A., Mihalopoulos, N., Violaki, K., Ingall, E.D., 2016. Influence of atmospheric processes on the solubility and composition of iron in saharan dust. Environ. Sci. Technol. 50 (13), 6912–6920. https://doi.org/10.1021/acs.est.6b02605.

Lucarelli, F., Calzolai, G., Chiari, M., Giannoni, M., Mochi, D., Nava, S., Carraresi, L., 2014. The upgraded external-beam PIXE/PIGE set-up at LABEC for very fast measurements on aerosol samples. Nucl. Instrum. Methods Phys. Res. Sect. B Beam Interact. Mater. Atoms 318, 55–59. https://doi.org/10.1016/j.nimb.2013.05.099.

Lucarelli, F., Calzolai, G., Chiari, M., Nava, S., Carraresi, L., 2018. Study of atmospheric aerosols by IBA techniques: the LABEC experience. Nucl. Instrum. Methods Phys. Res. Sect. B Beam Interact. Mater. Atoms 417, 121–127. https://doi.org/10.1016/j.nimb.2017.07.034.

Luo, C., Gao, Y., 2010. Aeolian iron mobilisation by dust - acid interactions and their implications for soluble iron deposition to the ocean: a test involving potential anthropogenic organic acidic species. Environ. Chem. 7 (2), 153. https://doi.org/10.1071/EN09116.

Mahowald, N., 2011. Aerosol indirect effect on biogeochemical cycles and climate. Science (80-.) 334 (6057), 794–796. https://doi.org/10.1126/science.1207374.

Mahowald, N.M., Hamilton, D.S., Mackey, K.R.M., Moore, J.K., Baker, A.R., Scanza, R.A., Zhang, Y., 2018. Aerosol trace metal leaching and impacts on marine microorganisms. Nat. Commun. 9 (1), 2614. https://doi.org/10.1038/s41467-018-04970-7.

Martínez-Garcia, A., Rosell-Melé, A., Geibert, W., Gersonde, R., Masqué, P., Gaspari, V., Barbante, C., 2009. Links between iron supply, marine productivity, sea surface temperature, and CO 2 over the last 1.1 Ma. Paleoceanography 24 (1). https://doi.org/10.1029/2008PA001657 n/a-n/a.

Mason, B., 1966. Principles of Geochemistry. Wiley, New York.

McDaniel, M.F.M., Ingall, E.D., Morton, P.L., Castorina, E., Weber, R.J., Shelley, R.U., Landing, W.M., Longo, A.F., Feng, Y., Lai, B., 2019. Relationship between atmospheric aerosol mineral surface area and iron solubility. ACS Earth Sp. Chem. 3 (11), 2443–2451. https://doi.org/10.1021/acsearthspacechem.9b00152.

Mead, C., Herckes, P., Majestic, B.J., Anbar, A.D., 2013. Source apportionment of aerosol iron in the marine environment using iron isotope analysis. Geophys. Res. Lett. 40 (21), 5722–5727. https://doi.org/10.1002/2013GL057713.

Meskhidze, N., 2003. Iron mobilization in mineral dust: can anthropogenic SO 2 emissions affect ocean productivity? Geophys. Res. Lett. 30 (21), 2085. https://doi.org/10.1029/2003GL018035.

Meskhidze, N., 2005. Dust and pollution: a recipe for enhanced ocean fertilization? J. Geophys. Res. 110 (D3), D03301. https://doi.org/10.1029/2004JD005082.

Meskhidze, N., Johnson, M.S., Hurley, D., Dawson, K., 2016a. Influence of measurement uncertainties on fractional solubility of iron in mineral aerosols over the oceans. Aeolian Res 22, 85–92. https://doi.org/10.1016/j.aeolia.2016.07.002.

Meskhidze, N., Johnson, M.S., Hurley, D., Dawson, K., 2016b. Influence of measurement uncertainties on fractional solubility of iron in mineral aerosols over the oceans. Aeolian Res 22, 85–92. https://doi.org/10.1016/j.aeolia.2016.07.002.

Meskhidze, N., Hurley, D., Royalty, T.M., Johnson, M.S., 2017. Potential effect of atmospheric dissolved organic carbon on the iron solubility in seawater. Mar. Chem. 194, 124–132. https://doi.org/10.1016/j.marchem.2017.05.011.

Moore, C.M., Mills, M.M., Arrigo, K.R., Berman-Frank, I., Bopp, L., Boyd, P.W., Galbraith, E.D., Geider, R.J., Guieu, C., Jaccard, S.L., Jickells, T.D., La Roche, J., Lenton, T.M., Mahowald, N.M., Marañón, E., Marinov, I., Moore, J.K., Nakatsuka, T., Oschlies, A., Saito, M.A., Thingstad, T.F., Tsuda, A., Ulloa, O., 2013. Processes and patterns of oceanic nutrient limitation. Nat. Geosci. 6 (9), 701–710. https://doi.org/10.1038/ngeo1765.

Morton, P.L., Landing, W.M., Hsu, S.-C., Milne, A., Aguilar-Islas, A.M., Baker, A.R., Bowie, A.R., Buck, C.S., Gao, Y., Gichuki, S., Hastings, M.G., Hatta, M., Johansen, A. M., Losno, R., Mead, C., Patey, M.D., Swarr, G., Vandermark, A., Zamora, L.M., 2013. Methods for the sampling and analysis of marine aerosols: results from the 2008

GEOTRACES aerosol intercalibration experiment. Limnol Oceanogr. Methods 11 (2), 62–78. https://doi.org/10.4319/lom.2013.11.62.

Na, K., Sawant, A.A., Song, C., Cocker, D.R., 2004. Primary and secondary carbonaceous species in the atmosphere of Western Riverside County, California. Atmos. Environ. 38 (9), 1345–1355. https://doi.org/10.1016/j.atmosenv.2003.11.023.

Nishioka, J., Takeda, S., Wong, C., Johnson, W., 2001. Size-fractionated iron concentrations in the northeast Pacific Ocean: distribution of soluble and small colloidal iron. Mar. Chem. 74 (2–3), 157–179. https://doi.org/10.1016/S0304-4203(01)00013-5.

Okochi, H., Brimblecombe, P., 2002. Potential trace metal–organic complexation in the atmosphere. Sci. World J. 2, 767–786. https://doi.org/10.1100/tsw.2002.132.

Paris, R., Desboeufs, K.V., Journet, E., 2011. Variability of dust iron solubility in atmospheric waters: investigation of the role of oxalate organic complexation. Atmos. Environ. 45 (36), 6510–6517. https://doi.org/10.1016/j.atmosenv.2011.08.068.

Paytan, A., Mackey, K.R.M., Chen, Y., Lima, I.D., Doney, S.C., Mahowald, N., Labiosa, R., Post, A.F., 2009. Toxicity of atmospheric aerosols on marine phytoplankton. Proc. Natl. Acad. Sci. Unit. States Am. 106 (12), 4601–4605. https://doi.org/10.1073/pnas.0811486106.

Pérez García-Pando, C., Miller, R.L., Perlwitz, J.P., Rodríguez, S., Prospero, J.M., 2016. Predicting the mineral composition of dust aerosols: insights from elemental composition measured at the Izaña Observatory. Geophys. Res. Lett. 43 (19), 10,520–10,529. https://doi.org/10.1002/2016GL069873.

Prospero, J.M., 1999. Long-term measurements of the transport of African mineral dust to the southeastern United States: implications for regional air quality. J. Geophys. Res. Atmos. 104 (D13), 15917–15927. https://doi.org/10.1029/1999JD900072.

Prospero, J.M., 2003. African droughts and dust transport to the caribbean: climate change implications. Science (80-.) 302 (5647), 1024–1027. https://doi.org/10.1126/science.1089915.

Prospero, J.M., Carlson, T.N., 1972. Vertical and areal distribution of Saharan dust over the western equatorial north Atlantic Ocean. J. Geophys. Res. 77 (27), 5255–5265. https://doi.org/10.1029/JC077i027p05255.

Raiswell, R., Hawkings, J.R., Benning, L.G., Albani, S., Mahowald, N., 2017. Comments on 'Influence of measurement uncertainties on fractional solubility of iron in mineral aerosols over the oceans' Aeolian Research 22, 85–92. Aeolian Res 25, 123–125. https://doi.org/10.1016/j.aeolia.2017.03.003.

Ravelo-Pérez, L.M., Rodríguez, S., Galindo, L., García, M.I., Alastuey, A., López-Solano, J., 2016. Soluble iron dust export in the high altitude Saharan Air Layer. Atmos. Environ. 133, 49–59. https://doi.org/10.1016/j.atmosenv.2016.03.030.

Reche, C., Querol, X., Alastuey, A., Viana, M., Pey, J., Moreno, T., Rodríguez, S., González, Y., Fernández-Camacho, R., de la Rosa, J., Dall&apos, Osto, M., Prévôt, A. S.H., Hueglin, C., Harrison, R.M., Quincey, P., 2011. New considerations for PM, Black Carbon and particle number concentration for air quality monitoring across different European cities. Atmos. Chem. Phys. 11 (13), 6207–6227. https://doi.org/10.5194/acp-11-6207-2011.

Ridgwell, A.J., Watson, A.J., 2002. Feedback between aeolian dust, climate, and atmospheric CO 2 in glacial time. Paleoceanography 17 (4), 11-1–11–11. https://doi.org/10.1029/2001PA000729.

Rodríguez, S., Cuevas, E., 2007. The contributions of "minimum primary emissions" and "new particle formation enhancements" to the particle number concentration in urban air. J. Aerosol Sci. 38 (12), 1207–1219. https://doi.org/10.1016/j.jaerosci.2007.09.001.

Rodríguez, S., Alastuey, A., Alonso-Pérez, S., Querol, X., Cuevas, E., Abreu-Afonso, J., Viana, M., Pérez, N., Pandolfi, M., de la Rosa, J., 2011. Transport of desert dust mixed with North African industrial pollutants in the subtropical Saharan Air Layer. Atmos. Chem. Phys. 11 (13), 6663–6685. https://doi.org/10.5194/acp-11-6663-2011.

Rodríguez, S., Alastuey, A., Querol, X., 2012. A review of methods for long term in situ characterization of aerosol dust. Aeolian Res 6, 55–74. https://doi.org/10.1016/j.aeolia.2012.07.004.

Rodríguez, S., Cuevas, E., Prospero, J.M., Alastuey, A., Querol, X., López-Solano, J., García, M.I., Alonso-Pérez, S., 2015. Modulation of saharan dust export by the North African dipole. Atmos. Chem. Phys. 15 (13), 7471–7486. https://doi.org/10.5194/acp-15-7471-2015.

Rodríguez, S., Prospero, J.M., López-Darias, J., García-Alvarez, M.I., Zuidema, P., Nava, S., Lucarelli, F., Gaston, C.J., Galindo, L., Sosa, E., 2020a. Aerosol Chemistry and Soluble Iron in Tenerife, Barbados and Miami in Summer 2015 - Dataset. https://doi.org/10.20350/digitalCSIC/12709.

Rodríguez, S., Calzolai, G., Chiari, M., Nava, S., García, M.I., López-Solano, J., Marrero, C., López-Darias, J., Cuevas, E., Alonso-Pérez, S., Prats, N., Amato, F., Lucarelli, F., Querol, X., 2020b. Rapid changes of dust geochemistry in the Saharan Air Layer linked to sources and meteorology. Atmos. Environ. 223, 117186. https://doi.org/10.1016/j.atmosenv.2019.117186.

Rubasinghege, G., Kyei, P.K., Scherer, M.M., Grassian, V.H., 2012. Proton-promoted dissolution of α-FeOOH nanorods and microrods: size dependence, anion effects (carbonate and phosphate), aggregation and surface adsorption. J. Colloid Interface Sci. 385 (1), 15–23. https://doi.org/10.1016/j.jcis.2012.06.049.

Rudnick, R.L., Gao, S., 2003. Composition of the Continental Crust. In: Treatise on Geochemistry. Elsevier, pp. 1–64.

Saito, M.A., Goepfert, T.J., Ritt, J.T., 2008. Some thoughts on the concept of colimitation: three definitions and the importance of bioavailability. Limnol. Oceanogr. 53 (1), 276–290. https://doi.org/10.4319/lo.2008.53.1.0276.

Scheuvens, D., Schütz, L., Kandler, K., Ebert, M., Weinbruch, S., 2013. Bulk composition of northern African dust and its source sediments — a compilation. Earth Sci. Rev. 116, 170–194. https://doi.org/10.1016/j.earscirev.2012.08.005.

Schroth, A.W., Crusius, J., Sholkovitz, E.R., Bostick, B.C., 2009. Iron solubility driven by speciation in dust sources to the ocean. Nat. Geosci. 2 (5), 337–340. https://doi.org/10.1038/ngeo501.

Schulz, M., Prospero, J.M., Baker, A.R., Dentener, F., Ickes, L., Liss, P.S., Mahowald, N. M., Nickovic, S., García-Pando, C.P., Rodríguez, S., Sarin, M., Tegen, I., Duce, R.A., 2012. Atmospheric transport and deposition of mineral dust to the ocean: implications for research needs. Environ. Sci. Technol. 46 (19), 10390–10404. https://doi.org/10.1021/es300073u.

Sedwick, P.N., Sholkovitz, E.R., Church, T.M., 2007. Impact of anthropogenic combustion emissions on the fractional solubility of aerosol iron: evidence from the Sargasso Sea. G-cubed 8 (10). https://doi.org/10.1029/2007GC001586 n/a-n/a.

Shi, Z., Krom, M.D., Bonneville, S., Baker, A.R., Jickells, T.D., Benning, L.G., 2009. formation of iron nanoparticles and increase in iron reactivity in mineral dust during simulated cloud processing. Environ. Sci. Technol. 43 (17), 6592–6596. https://doi.org/10.1021/es901294g.

Shi, Z., Krom, M.D., Jickells, T.D., Bonneville, S., Carslaw, K.S., Mihalopoulos, N., Baker, A.R., Benning, L.G., 2012. Impacts on iron solubility in the mineral dust by processes in the source region and the atmosphere: a review. Aeolian Res 5, 21–42. https://doi.org/10.1016/j.aeolia.2012.03.001.

Sholkovitz, E.R., Sedwick, P.N., Church, T.M., 2009. Influence of anthropogenic combustion emissions on the deposition of soluble aerosol iron to the ocean: empirical estimates for island sites in the North Atlantic. Geochem. Cosmochim. Acta 73 (14), 3981–4003. https://doi.org/10.1016/j.gca.2009.04.029.

Sholkovitz, E.R., Sedwick, P.N., Church, T.M., Baker, A.R., Powell, C.F., 2012. Fractional solubility of aerosol iron: synthesis of a global-scale data set. Geochem. Cosmochim. Acta 89, 173–189. https://doi.org/10.1016/j.gca.2012.04.022.

Sippula, O., Hokkinen, J., Puustinen, H., Yli-Pirilä, P., Jokiniemi, J., 2009. Comparison of particle emissions from small heavy fuel oil and wood-fired boilers. Atmos. Environ. 43 (32), 4855–4864. https://doi.org/10.1016/j.atmosenv.2009.07.022.

Stein, A.F., Draxler, R.R., Rolph, G.D., Stunder, B.J.B., Cohen, M.D., Ngan, F., 2015. NOAA's HYSPLIT atmospheric transport and dispersion modeling system. Bull. Am. Meteorol. Soc. 96 (12), 2059–2077. https://doi.org/10.1175/BAMS-D-14-00110.1.

Taylor, S.R., Mclennan, S., 1985. The Continental Crust : its Composition and Evolution : an Examination of the Geochemical Record Preserved in Sedimentary Rocks. United States.

Taylor, S.R., 1964. The abundance of chemical elements in the continental crust- a new table. Geochem. Cosmochim. Acta 28, 1273–1285.

Theodosi, C., Markaki, Z., Mihalopoulos, N., 2010. Iron speciation, solubility and temporal variability in wet and dry deposition in the Eastern Mediterranean. Mar. Chem. 120 (1–4), 100–107. https://doi.org/10.1016/j.marchem.2008.05.004.

Trapp, J.M., Millero, F.J., Prospero, J.M., 2010a. Temporal variability of the elemental composition of African dust measured in trade wind aerosols at Barbados and Miami. Mar. Chem. 120 (1–4), 71–82. https://doi.org/10.1016/j.marchem.2008.10.004.

Trapp, J.M., Millero, F.J., Prospero, J.M., 2010b. Trends in the solubility of iron in dust-dominated aerosols in the equatorial Atlantic trade winds: importance of iron speciation and sources. G-cubed 11 (3). https://doi.org/10.1029/2009GC002651 n/a-n/a.

Tsamalis, C., Chédin, A., Pelon, J., Capelle, V., 2013. The seasonal vertical distribution of the Saharan Air Layer and its modulation by the wind. Atmos. Chem. Phys. 13 (22), 11235–11257. https://doi.org/10.5194/acp-13-11235-2013.

Turpin, B.J., Huntzicker, J.J., 1995. Identification of secondary organic aerosol episodes and quantitation of primary and secondary organic aerosol concentrations during SCAQS. Atmos. Environ. 29 (23), 3527–3544. https://doi.org/10.1016/1352-2310(94)00276-Q.

Wang, R., Balkanski, Y., Boucher, O., Bopp, L., Chappell, A., Ciais, P., Hauglustaine, D., Peñuelas, J., Tao, S., 2015. Sources, transport and deposition of iron in the global atmosphere. Atmos. Chem. Phys. 15 (11), 6247–6270. https://doi.org/10.5194/acp-15-6247-2015.

Wiederhold, J.G., Kraemer, S.M., Teutsch, N., Borer, P.M., Halliday, A.N., Kretzschmar, R., 2006. Iron isotope fractionation during proton-promoted, ligand-controlled, and reductive dissolution of goethite. Environ. Sci. Technol. 40 (12), 3787–3793. https://doi.org/10.1021/es052228y.

Wozniak, A.S., Shelley, R.U., Sleighter, R.L., Abdulla, H.A.N., Morton, P.L., Landing, W. M., Hatcher, P.G., 2013. Relationships among aerosol water soluble organic matter, iron and aluminum in European, North African, and Marine air masses from the 2010 US GEOTRACES cruise. Mar. Chem. 154, 24–33. https://doi.org/10.1016/j.marchem.2013.04.011.

Wozniak, A.S., Shelley, R.U., McElhenie, S.D., Landing, W.M., Hatcher, P.G., 2015. Aerosol water soluble organic matter characteristics over the North Atlantic Ocean: implications for iron-binding ligands and iron solubility. Mar. Chem. 173, 162–172. https://doi.org/10.1016/j.marchem.2014.11.002.

Zamora, L.M., Prospero, J.M., Hansell, D.A., 2011. Organic nitrogen in aerosols and precipitation at Barbados and Miami: implications regarding sources, transport and deposition to the western subtropical North Atlantic. J. Geophys. Res. 116 (D20), D20309. https://doi.org/10.1029/2011JD015660.

Zamora, L.M., Prospero, J.M., Hansell, D.A., Trapp, J.M., 2013. Atmospheric P deposition to the subtropical North Atlantic: sources, properties, and relationship to N deposition. J. Geophys. Res. Atmos. 118 (3), 1546–1562. https://doi.org/10.1002/jgrd.50187.

Zuidema, P., Alvarez, C., Kramer, S.J., Custals, L., Izaguirre, M., Sealy, P., Prospero, J.M., Blades, E., 2019. Is summer African dust arriving earlier to Barbados? The updated long-term in situ dust mass concentration time series from ragged point, Barbados, and Miami, Florida. Bull. Am. Meteorol. Soc. 100 (10), 1981–1986. https://doi.org/10.1175/BAMS-D-18-0083.1.